Influence of the high-temperature "firing" step on high-rate plasma deposited silicon nitride films used as bulk passivating antireflection coatings on silicon solar cells

Influence of the high-temperature "firing" step on high-rate plasma deposited silicon nitride films used as bulk passivating antireflection coatings on silicon solar cells

J. Hong and W. M. M. Kessels[a)]
Department of Applied Physics, Eindhoven University of Technology, P.O. Box 513, 5600 MB Eindhoven, The Netherlands

W. J. Soppe and A. W. Weeber
ECN Solar Energy, P.O. Box 1, 1755 ZG Petten, The Netherlands

W. M. Arnoldbik
Surfaces, Interfaces and Devices, Debye Institute, Utrecht University, P.O. Box 80.000, 3508 TA Utrecht, The Netherlands

M. C. M. van de Sanden[b)]
Department of Applied Physics, Eindhoven University of Technology, P.O. Box 513, 5600 MB Eindhoven, The Netherlands

(Received 11 March 2003; accepted 21 July 2003; published 15 September 2003)

The influence of a short high-temperature step, comparable to the so-called ''firing'' of the metallization on silicon solar cells, on properties of high-rate (>0.5 nm/s) plasma deposited silicon nitride (a-SiN_x:H) films has been investigated. These a-SiN_x:H films are used as antireflection coating on multicrystalline silicon (mc-Si) solar cells and, after the firing process, they also induce hydrogen bulk passivation in the mc-Si. Three different types of remote plasma deposited a-SiN_x:H films have been investigated: (i) expanding thermal plasma (ETP) deposited a-SiN_x:H films from a N_2-SiH_4 gas mixture, (ii) ETP deposited a-SiN_x:H films from a NH_3-SiH_4 mixture, and (iii) microwave plasma deposited a-SiN_x:H films from a NH_3-SiH_4 mixture. The atomic composition and optical and structural properties of the films have been studied before and after the high-temperature step by the combination of elastic recoil detection, spectroscopic ellipsometry, and Fourier transform infrared spectroscopy. It has been observed that the high-temperature step can induce significant changes in hydrogen content, bonding types, mass density, and optical absorption of the films. These thermally induced effects are more enhanced for Si- than for N-rich films, which in some cases have a high thermal stability. Furthermore, the material properties and the influence of the high-temperature step have been related to the bulk passivation properties of the a-SiN_x:H coated mc-Si solar cells. It is found that in particular the density and thermal stability of the a-SiN_x:H films seem to be important for the degree of the bulk passivation obtained. © *2003 American Vacuum Society.* [DOI: 10.1116/1.1609481]

I. INTRODUCTION

Along with a traditional wide range of applications in microelectronics,[1,2] silicon nitride (a-SiN_x:H) films deposited by plasma enhanced chemical vapor deposition (PECVD) have recently also gained deep interest from the photovoltaics industry. The application of a-SiN_x:H films is regarded as one of the most promising antireflection (AR) and defect and impurity passivation schemes for solar cells based on low-cost silicon materials, such as multicrystalline silicon (mc-Si) and Si ribbons.[3] Plasma deposited a-SiN_x:H films are well suited to reduce reflection losses of light incident on Si solar cells due to the combination of a good optical transparency with a tunable refractive index,[4,5] but at the same time also a variety of electronic defects (intrinsic or extrinsic) of mc-Si can be passivated by applying a high-temperature step to the a-SiN_x:H layer. When passivated, these defects do not act as recombination traps for photogenerated minority charge carriers within the Si band gap. Furthermore, a-SiN_x:H films can also lead to efficient reduction of recombination losses at the surface of the Si solar cells (i.e., surface passivation).

A number of studies have been devoted to elucidate the underlying mechanisms of surface and bulk passivation of Si solar cells as induced by a-SiN_x:H.[6–18] Bulk passivation can be achieved by a short high-temperature step, the so-called firing process, which is used for the application of screen-printed metallization of a-SiN_x:H coated mc-Si solar cells. During this firing process, defect passivation in Si is obtained by hydrogen species that are released from the a-SiN_x:H film and that diffuse into Si. In several studies, models have been proposed for the diffusion of these hydrogen species into silicon in the form of atomic hydrogen (H), molecular hydrogen (H_2), and ammonia (NH_3).[10,11] Furthermore, vacancy–hydrogen complex generation and Al-enhanced void generation have been suggested to occur dur-

a)Electronic mail: w.m.m.kessels@tue.nl
b)Electronic mail: m.c.m.v.d.sanden@tue.nl

ing the firing process of screen-printed Al-based contacts.[12–16] Furthermore, the retention of the atomic hydrogen at defect sites during the rapid cooling of the cells immediately after the firing process to obtain enhanced passivation effects has been considered.[15,16]

An important issue for the application of a-SiN_x:H films in the photovoltaic industry is the deposition rate of the a-SiN_x:H. Increasing the deposition rate is a real challenge in large-scale solar cell production because at higher deposition rates investments in equipment can be kept relatively low reducing the costs per wafer processed. In our recent work,[17,18] the expanding thermal plasma (ETP) technique has been shown to provide bulk passivating a-SiN_x:H layers at high deposition rates. These deposition rates of the ETP a-SiN_x:H films are in the range of 1–20 nm/s and are much higher than those of a-SiN_x:H deposited by conventional PECVD methods (typically, 0.1 nm/s).[19] The ETP technique belongs to the class of remote PECVD techniques with as major advantages over the direct plasma techniques: (i) independent control of the processes in the downstream region, (ii) decoupling of the plasma parameters, (iii) and almost no ion bombardment on the substrate. Ion bombardment can, however, be applied by the application of an external bias voltage to the substrate.

Although significant progress has been made recently in terms of passivation of solar cells by plasma deposited a-SiN_x:H films, there is still no complete understanding of the mechanism of bulk passivation by a-SiN_x:H for mc-Si solar cells. This is partially due to an insufficient understanding of the fundamental properties of the a-SiN_x:H that affect hydrogen release and hydrogen diffusion into mc-Si, such as the atomic composition, microstructure, density, and hydrogen bonding types. Especially, the dependence of the bulk passivation on these a-SiN_x:H properties has not been addressed in detail. The motivation for the work presented in this article is, therefore, to study how a-SiN_x:H film properties are related to the degree of bulk passivation obtained after the firing process. In particular, a-SiN_x:H films deposited by remote plasmas at high deposition rates have been investigated: (i) a-SiN_x:H films deposited by the ETP technique from a N_2-SiH_4 gas mixture (deposition rate is $\sim$8 nm/s); (ii) a-SiN_x:H films deposited by the ETP technique from a NH_3-SiH_4 mixture ($\sim$4 nm/s); and (iii) a-SiN_x:H films deposited by a remote microwave (MW) plasma operated on a NH_3-SiH_4 mixture ($\sim$0.7 nm/s). To examine the influence of the firing process, the compositional and optical properties of the films have been systematically studied before and after a high-temperature step that mimics the heat treatment of the film during the firing process. The film diagnostics used are elastic recoil detection (ERD) analysis, spectroscopic ellipsometry (SE), and Fourier transform infrared (FTIR) spectroscopy.

II. EXPERIMENTAL DETAILS

A. Film preparation and high-temperature step

Silicon nitride films have been prepared by two different remote plasma deposition techniques. The expanding thermal plasma has been used for the preparation of a-SiN_x:H films at the Eindhoven University of Technology while the MW PECVD technique has been employed at the Energy research Center of the Netherlands (ECN). Three different types of a-SiN_x:H films have been investigated for comparison purposes: (i) ETP deposited a-SiN_x:H films deposited from a N_2-SiH_4 gas mixture, (ii) ETP deposited a-SiN_x:H films deposited from a NH_3-SiH_4 mixture, (iii) and MW deposited a-SiN_x:H films deposited from a NH_3-SiH_4 mixture. For convenience, these three types of a-SiN_x:H films will be referred to as "ETP N_2," "ETP NH_3," and "MW NH_3" films, respectively.

The ETP deposition system has been extensively described in the literature,[19–21] and it will be described only briefly here. In a cascaded arc plasma source, a thermal plasma is generated at subatmospheric pressure ($\sim$40 kPa) by running a dc current through a small plasma channel operated on pure Ar (when using NH_3) or a mixture of $Ar-N_2-H_2$ (when using N_2). Driven by a large pressure gradient, this nondepositing plasma expands into a low-pressure ($\sim$20 Pa) downstream deposition chamber. In this downstream region, a mixture of NH_3-SiH_4 or pure SiH_4 is injected into the plasma expansion region when working with NH_3 or N_2, respectively.

The resulting reaction products, which are created by the interaction of reactive species emanating from the plasma source, deposit on the substrate holder located at a distance of 70 cm from the plasma source. This specific plasma source to substrate distance was chosen because it yields a reasonable uniform film thickness on a substrate area of 100 cm^2.[19]

Substrates can be placed at the substrate holder which is made of aluminum and positioned on a yoke. The yoke can be heated up to 500 °C using Ohmic heating. The substrate temperature was maintained at 350 °C for the deposition of the a-SiN_x:H films presented in this study. The thermal contact between the yoke, substrate holder, and substrate is optimized by a He backflow, leading to a maximum temperature difference of 15 °C between the yoke and substrate.[19] A wide range of ETP a-SiN_x:H films, from N rich to Si rich and with different hydrogen concentrations, has been prepared using different plasma operating conditions. The gas flows and other discharge parameters for the ETP deposited a-SiN_x:H films from N_2-SiH_4 and NH_3-SiH_4 gas mixtures are given in Table I. The corresponding deposition rates are, typically, $\sim$8 and $\sim$4 nm/s for the ETP N_2 and ETP NH_3 films, respectively.

The MW remote PECVD system at ECN has been developed in cooperation between ECN and the company Roth & Rau and has been reported on previously.[22–24] The in-line system at ECN, which consists of loadlock and preheating and cooling compartments, is capable of processing 150 wafers (10×10 cm^2 size) per hour in a continuous process. The plasma source is situated in the middle compartment of the reactor and consists of a quartz tube with a Cu antenna inside. The source, operating at a microwave frequency of 2.45 GHz, includes an arrangement of permanent magnets for

TABLE I. Plasma conditions used for the deposition of a-SiN_x:H films by the ETP technique using N_2 ("ETP N_2") and NH_3 ("ETP NH_3") as N-containing precursor gas. The total flow rates of the N-containing and Si-containing precursor gases have been kept constant at 18 sccs (standard cm^3/s).

	ETP N_2	ETP NH_3
Ar flow (sccs)	55	55
H_2 flow (sccs)	5	0
N_2 flow (sccs)	1–17	···
NH_3 flow (sccs)	···	15–17
SiH_4 flow (sccs)	1–17	1–3
Downstream pressure (Pa)	18–20	18–20
Cascaded arc current (A)	45	45
Cascaded arc voltage (V)	210	70

electron confinement in the plasma. The plasma is operated on NH_3, which is injected close to the quartz tube. In the downstream region, SiH_4 is injected into the plasma. The a-SiN_x:H films presented in this article have been deposited at a substrate temperature of 350 °C and in the pressure range 2–30 Pa. Some of these conditions have systematically been optimized to obtain a-SiN_x:H films with optimum bulk passivation performance. Table II gives the pressure and flow ratio used for the MW deposited a-SiN_x:H films. The deposition rate is, typically, 0.7–1.0 nm/s.

The substrates used for both the ETP and MW deposited a-SiN_x:H films are 2.5×2.5 cm^2 pieces of monocrystalline silicon wafers (100, float zone (FZ), p type, 500 μm thick, 10–20 Ω cm) covered with approximately 2-nm-thick native oxide. For each deposition condition, two a-SiN_x:H samples have been prepared in one deposition run. One of the samples has undergone the high-temperature step, while the other sample is analyzed as deposited for comparison purposes. The high-temperature step has taken place in an infrared lamp heated belt furnace at ECN, which is also used for the firing process of screen-printed metallization of the mc-Si solar cells. The furnace temperature (700–800 °C) and operating time (less than 1 min) is specifically optimized for solar cells coated with a-SiN_x:H deposited with the remote MW plasma.

B. Film analysis

The composition of the a-SiN_x:H films as well as the areal density (expressed in atoms/cm^2) of the different type of atoms present in the material, has been determined by heavy ion ERD analysis at Utrecht University.[25] For these measurements a 54 MeV $^{65}Cu^{8+}$ beam was directed at the sample under an angle of 20° with the surface. The beam spot on the samples was approximately 12 mm^2 (3 mm $\times$4 mm) for all measurements. Particles recoiled from the sample at an angle of 30° with the incoming beam were identified and energy analyzed by means of an ionization chamber. The resulting energy spectra were converted into concentration depth profiles of the elements present in the sample. Special care has been given to hydrogen. In the case of large hydrogen concentrations, hydrogen tends to desorb from the layers under heavy ion irradiation.[26] Therefore, the hydrogen concentrations were determined in a separate measurement using a solid state detector with a large opening angle. During this measurement the hydrogen content in the film was monitored as a function of ion dose and extrapolated to its initial value. The atomic density of the films has been quantified by dividing the areal density from ERD by the thickness of the films as determined by spectroscopic ellipsometry. The inaccuracies in the atomic densities and concentrations are less than 5%.

TABLE II. Pressure and gas flow ratio R [$=NH_3/(SiH_4+NH_3)$] for the MW deposited a-SiN_x:H films ("MW NH_3").

Sample No.	p (Pa)	R
1	2	0.62
2	10	0.62
3	30	0.62
4	10	0.52

The optical and infrared vibrational properties of the a-SiN_x:H films have been examined by ultraviolet–visible SE and FTIR absorption spectroscopy. The spectroscopic ellipsometer used is a rotating-compensator type of instrument (J.A. Woollam, M-2000U), which measures the ellipsometric spectra in the wavelength range 245–1000 nm with the resolution of 470 wavelengths. From the spectroscopic ellipsometric data, the wavelength-dependent optical constants (the refractive index n and extinction coefficient k) and the film structure have been determined by optical modeling.[27–29] The Tauc–Lorentz dispersion model proposed by Jellison and Modine[27] has been adopted to describe the spectroscopic optical constants of the a-SiN_x:H films. Despite the complex mathematical description, the parametrization equation requires only four parameters and is well suited to fit optical functions of a variety of amorphous materials such as a-Si:H and a-SiN_x:H.[27] For the SE data analysis, we used a multiple layer model consisting of (i) ambient; (ii) a surface a-SiN_x:H layer (50% void+50% bulk a-SiN_x:H); (iii) bulk a-SiN_x:H layer; (iv) native oxide (SiO_2); and (v) monocrystalline Si substrate. The thickness of each layer and the dispersion parameters have been determined simultaneously by a nonlinear regression method in the analysis software. Prior to the measurements, a bare silicon substrate has been measured to define the thickness of the native oxide layer and the angle of incidence of the measurements. An initial guess for the dispersion model parameters has been extracted from the values reported for amorphous silicon nitride in the literature.[4,27] The error bars for the optical data are, typically, within the symbols of the data points for the figures presented.

The information on the hydrogen content and its bonding configurations has been obtained by infrared absorption spectroscopy using a Fourier transform infrared spectrometer (Bruker Vector 22) with a resolution of 4 cm^{-1}. The measurements were performed at normal incidence to the substrate. The substrate transmittance spectrum was measured before deposition and the transmittance spectrum of the combination "substrate film" was measured immediately after

deposition on the same spot. This procedure gives a reliable background for the transmittance spectrum in order to extract the absorbance of the film. The absorption coefficient of the a-SiN_x:H film was deduced from the spectrum taking into account the fringes caused by interference in the film as has been described in Ref. 30. The values of the film thickness that can be obtained by this method are in good agreement with those determined by SE. From the infrared absorption coefficient, the integrated absorption intensity I of the absorption bands has been calculated by the relationship[31]

$$I=\int \alpha(\omega)/\omega d\omega, \tag{1}$$

in which $\alpha(\omega)$ is the absorption coefficient and ω the infrared frequency. The effective peak frequency ω_{eff} of the absorption bands has been calculated as the center of gravity of the bands using the equation[32]

$$\omega_{\text{eff}}=\frac{\int \alpha(\omega)\omega d\omega}{\int \alpha(\omega) d\omega}. \tag{2}$$

III. COMPOSITIONAL AND OPTICAL FILM PROPERTIES

A. Properties of the as-deposited films

1. ETP deposited a-SiN_x:H films from N_2-SiH_4 and NH_3-SiH_4

Silicon nitride films have been deposited by the ETP technique under the conditions described in Table I, using different N-containing versus Si-containing precursor gas flow ratios R with $R=[N_2]/([N_2]+[SiH_4])$ or $R=[NH_3]/([NH_3]+[SiH_4])$. The composition and optical parameters of the ETP a-SiN_x:H films deposited from the N_2-SiH_4 plasma (ETP N_2) and the NH_3-SiH_4 plasma (ETP NH_3) as a function of the flow ratio R are shown in Figs. 1 and 2, respectively. For both types of the films, the [N]/[Si] ratio increases with increasing R. This is a common behavior of the plasma deposited a-SiN_x:H films. However, the ETP N_2 films show a substoichiometric [N]/[Si] ratio even at high values of R while the ETP NH_3 films show a stoichiometric composition at high R.

The hydrogen concentration in the films shows no clear dependence on R. The H content is in the range of 14–22 at. % for the ETP N_2 films, and in the range of 16–19 at. % for the ETP NH_3 films. Striking is the presence of a significant amount of oxygen atoms (6–27 at. %) in the ETP N_2 films. These oxygen atoms are incorporated after deposition when the films are exposed to air. This is concluded from the low oxygen concentration for the ETP NH_3 films and for ETP N_2 films deposited at shorter plasma source–substrate distances.[19] Furthermore, the base pressure in the ETP reactor is 10^{-4} Pa while pumped with a 450 l/s turbopump. Post-deposition oxidation has been also reported for rf PECVD a-SiN_x:H films deposited at low temperature.[33] It should be mentioned that the given concentrations are taken from the bulk region of the ERD depth profiles. The ETP NH_3 films as shown in Fig. 2 contain a much lower bulk concentration of oxygen, while some additional oxygen is detected on the surface of the samples. Permeation of the ambient oxygen species into the bulk reflects a porous microstructure of the ETP N_2 films. This indicates structural differences between the two types of the films deposited from N_2-SiH_4 and NH_3-SiH_4, which are formed by different gas-phase chem-

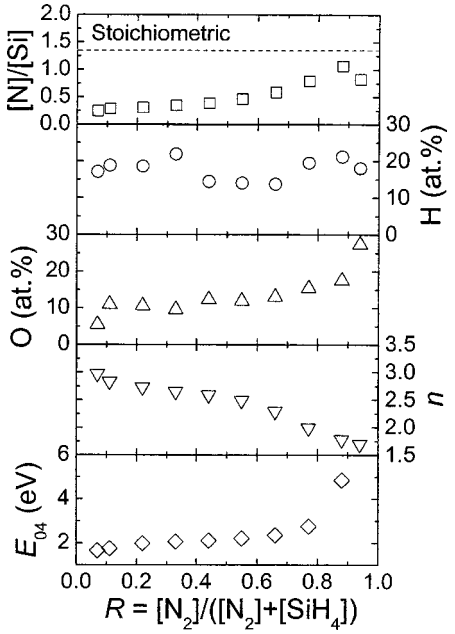

FIG. 1. Ratio N/Si, the H and O concentration, refractive index n measured at 2 eV, and optical band gap E_{04} of the ETP deposited a-SiN_x:H films from a N_2-SiH_4 mixture. The films were deposited by varying the relative N_2 and SiH_4 gas ratio, $R=[N_2]/([N_2]+[SiH_4])$.

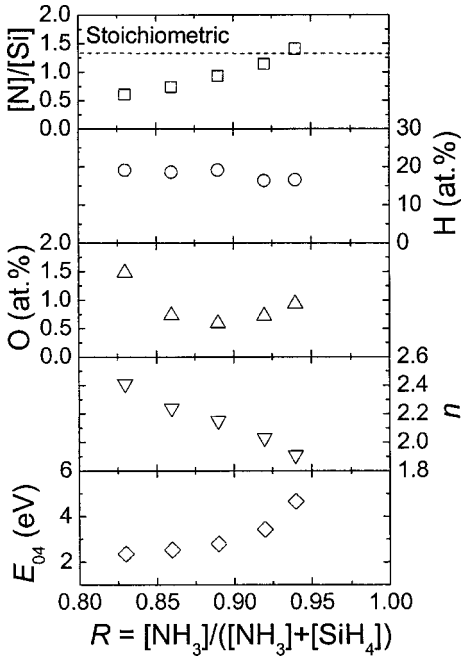

FIG. 2. The ratio N/Si, the H and O concentration, refractive index n measured at 2 eV, and optical band gap E_{04} of the ETP deposited a-SiN_x:H films from a NH_3-SiH_4 mixture. The films were deposited by varying the relative NH_3 and SiH_4 gas ratio, $R=[NH_3]/([NH_3]+[SiH_4])$.

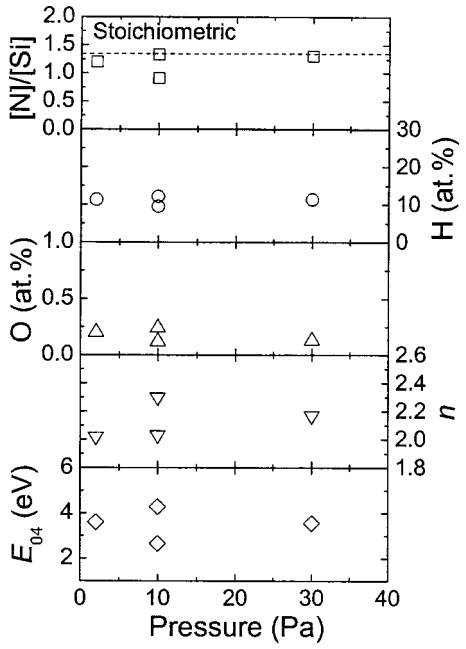

FIG. 3. The ratio N/Si, the H and O concentration, refractive index n measured at 2 eV, and optical band gap E_{04} of the MW deposited a-SiN_x:H films from a NH_3–SiH_4 mixture. The films were deposited at different pressures with various mixtures of NH_3 and SiH_4.

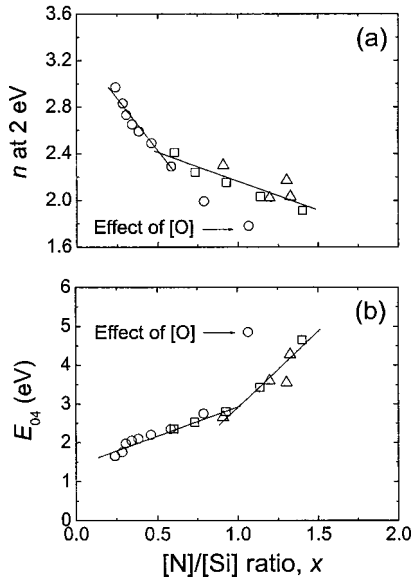

FIG. 4. (a) Refractive index n measured at 2 eV and (b) optical band gap E_{04} as a function of the [N]/[Si] ratio x of three types of a-SiN_x:H films. The solid lines are guides to the eye. (○ ETP N_2, □ ETP NH_3, and △ MW NH_3).

istries and by different plasma–surface interactions as investigated in the literature.[34–37]

The optical properties as shown in Figs. 1 and 2 are found to be fully tunable by the film composition, which itself is controlled by the flow ratio R. As R increases, the refractive index n decreases while the optical band gap E_{04} (defined as the energy where the absorption coefficient equals 10^4 cm^{-1}) increases. The variation of the optical constants as a function of R implies structural changes in the film from semiconducting-like (low-band-gap and high-absorption) Si-rich films to dielectric (high-band-gap and low-absorption) N-rich films for the ETP N_2 and ETP NH_3 films as shown in Figs. 1 and 2. The fact that the optical properties of the a-SiN_x:H films are tunable over a wide range is very important for optoelectronic applications.

2. MW deposited a-SiN_x:H from NH_3/SiH_4

The MW NH_3 films have been deposited under the conditions described in Table II. Figure 3 shows the composition and optical parameters of the MW NH_3 films as a function of pressure in the in-line deposition reactor. It is observed that the pressure does not significantly influence the properties of the films obtained, except for one film that is deposited at 10 Pa and with a higher SiH_4 partial pressure. The hydrogen content of the MW NH_3 films is slightly higher than 10 at. % and is much lower than those of the ETP films as shown in Figs 1 and 2. Furthermore, almost no oxygen contamination was observed (<0.2 at. %). This implies a higher density for the MW NH_3 films compared to the films deposited by the ETP technique.

3. Material properties versus the [N]/[Si] ratio of the a-SiN_x:H films

To investigate and compare the material properties of the three types of a-SiN_x:H films, the film properties are considered as a function of the [N]/[Si] ratio x of the a-SiN_x:H films. Figure 4 gives the variation of the refractive index n (at 2 eV) and the optical band gap E_{04} determined by SE as a function of x. It is observed that both n and E_{04} show a clear dependence on x and that the optical properties of the a-SiN_x:H films are actually determined by this parameter. However, for some values of x the refractive index n of the ETP N_2 films drops lower than expected on the basis of n of the ETP NH_3 and the MW NH_3 films. This can be attributed to the presence of a considerable amount of oxygen in the films. Since the refractive index of silicon oxide ($\sim$1.46) is generally lower than that of a-SiN_x:H, the incorporation of oxygen reduces the refractive index of a-SiN_x:H compared to the nominal value. Furthermore, for the MW NH_3 films, n is found to be slightly higher than that of the ETP NH_3 films, while E_{04} is lower. These observations are most probably associated with the higher density of the MW NH_3 films in comparison with the ETP NH_3 and ETP N_2 films, as will be addressed below.

Figure 5 shows the variation of the integrated intensity of the Si–N absorption bands [calculated by Eq. (1)] and the effective peak frequency of Si–H absorption bands [calculated by Eq. (2)] as a function of x for the three types of the a-SiN_x:H films. It is observed that the intensity of the Si–N absorption increases as x increases in the Si-rich regime ($x<1.0$) and seems to saturate when x approaches the stoichiometric value of $x=\sim$1.33. A similar behavior has been reported in the literature for rf PECVD deposited a-SiN_x:H films[32] and can be attributed to the fact that the number of

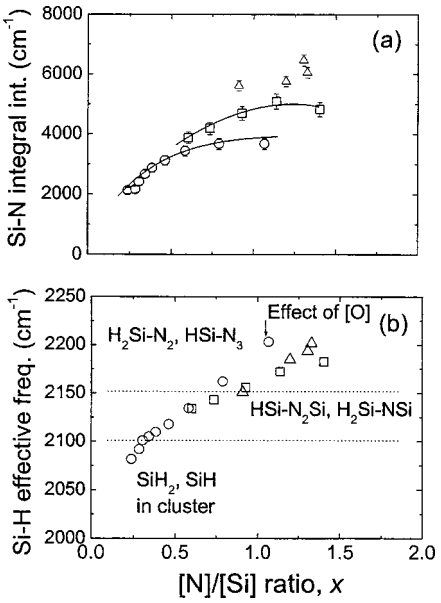

FIG. 5. (a) Integrated intensity of the Si–N stretching bands and (b) effective frequency of the Si–H bands as a function of the [N]/[Si] ratio x of three types of a-SiN_x:H films. Solid lines are guide to the eye. (○ ETP N_2, □ ETP NH_3, and △ MW NH_3).

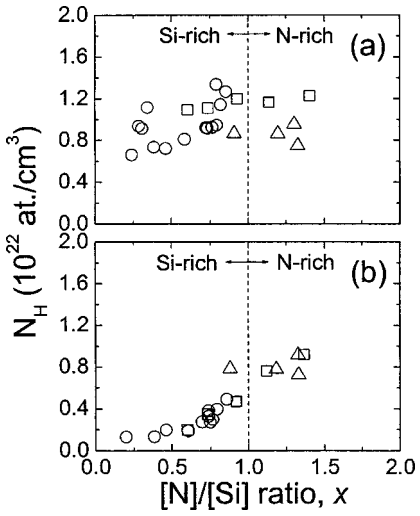

FIG. 6. Changes in hydrogen atomic density of the three types of a-SiN_x:H films as a function of the [N]/[Si] ratio x before (a) and after (b) the high-temperature step (○ ETP N_2, □ ETP NH_3, and △ MW NH_3).

Si–N bonds are maximized for stoichiometric films. However, the Si–N absorption intensity decreases when going from MW NH_3 to ETP NH_3 to ETP N_2 for one constant value of x. This can be attributed again to the lower density of the ETP NH_3 and ETP N_2 films compared to the MW NH_3 films causing a lower areal density of Si and N atoms as revealed by ERD.

Information on the hydrogen bonding configuration in a-SiN_x:H films has been obtained from infrared analysis[31] by considering the shift in the effective absorption frequencies of the Si–H stretching mode as shown in Fig. 5(b). Figure 5(b) shows that the effective frequency of the Si–H stretching mode shifts to higher wave numbers as x increases. This indicates a structural modification in local bonding configuration from Si- to N-rich a-SiN_x:H because the frequency of the Si–H mode shifts to higher wave numbers when the mean electronegativity of the backbonded atoms increases due to substitution of Si by N.[38] For some of the ETP N_2 films this shift is even more pronounced than for the ETP NH_3 films at $x=\sim 1.0$. This can be attributed to the presence of O atoms which have higher electronegativity than N atoms.

B. Influences of the high-temperature process step

1. Compositional properties

After the high-temperature step several changes in the composition of the a-SiN_x:H films have been observed in reference to the as-deposited films. Probably the most interesting observation with respect to the application of the a-SiN_x:H films for solar cell antireflection coatings is the decrease in H atomic density of the films and the resulting passivation of the underlying Si material. Figure 6 shows the change in the hydrogen quantity before (a) and after (b) the high-temperature process as a function of the [N]/[Si] ratio x of the films. The [N]/[Si] ratio itself is not affected by the high temperature step although the atomic densities of both Si and N increase slightly. This reveals that only H is released from the film leading to densification of the film as is discussed below. The amount of hydrogen released has however a strong dependence on the [N]/[Si] ratio of the a-SiN_x:H films. In the Si-rich region ($x<1.0$) much more H is released than in the N-rich region ($x>1.0$) in which the H release is relatively small and in some cases not even measurable. This behavior can be related to the difference in bond strength of the Si–H (~3.1 eV) and N–H (~4.1 eV) bonds in the a-SiN_x:H films.[39] The change from Si–H to N–H bonds as most abundant bonding type when going from Si- to N-rich films is observed by the infrared absorption measurements that reveal also clearly the influence of the high temperature step. Figure 7 shows the FTIR absorption spectra of the a-SiN_x:H films before and after the high-temperature process step. For comparison purposes, samples with a similar value of the refractive index, i.e., $n=\sim 2.1$, have been chosen for the three different techniques. The material properties of these three films are summarized in Table III. The spectra clearly show that the high-temperature step reduces the hydrogen content in the films. The hydrogen bonds, represented by the Si–H_x (~2000–2250 cm^{-1}) and N–H_x (NH~3340 cm^{-1} and NH_2 at ~3450 cm^{-1}) stretching modes, break during the high-temperature step and decrease the integrated intensities of the absorption modes. Figure 7 also shows that the ETP N_2 film experiences the largest loss of H while the H loss in the ETP NH_3 film is much less pronounced. Striking is, however, that the release of bonded hydrogen for the MW NH_3 film is almost negligible as almost no change in hydrogen quantity (within the experimental error) is observed for the MW NH_3 film. This can once again be attributed to the difference in the film density for these three types of a-SiN_x:H films.

The release of H due to the high temperature is associated

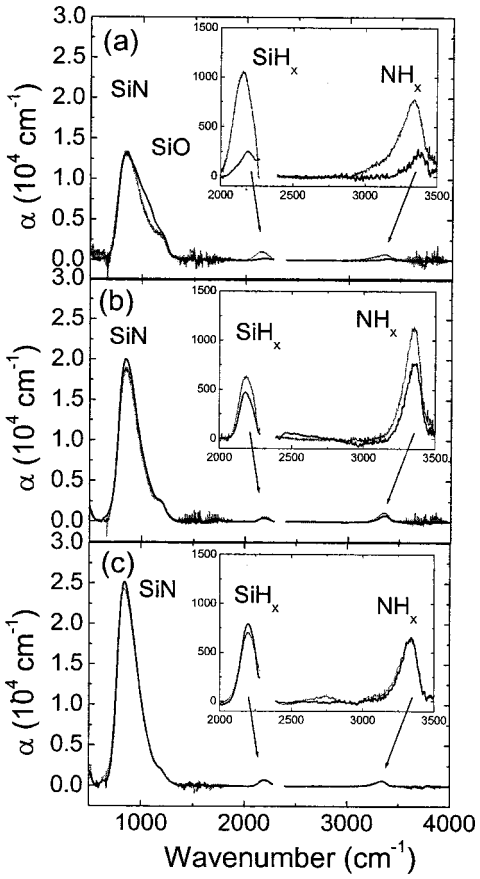

FIG. 7. FTIR absorption spectra of three types of a-SiN_x:H films before (gray) and after (black) the high-temperature step: (a) ETP N_2, (b) ETP NH_3, and (c) MW NH_3 film.

by a reconstruction of the film network by reactions such as

$$\mathrm{Si{-}H}(s)+\mathrm{N{-}H}(s)\rightarrow \mathrm{Si{-}N}(s)+\mathrm{H_2}(g), \tag{3}$$

$$\mathrm{Si{-}H}(s)+\mathrm{N{-}H_2}(s)\rightarrow \mathrm{Si{-}N}(s)+\mathrm{NH_3}(g), \tag{4}$$

as proposed by Lu *et al.*[40] The release of H in the form of H_2 or NH_3 has been reported in mass spectrometry studies during anneal studies.[35,41] An enhancement of the Si–N ($\sim$700–1020 cm^{-1}) stretching mode after the high temperature step is also observed for the ETP NH_3 and MW NH_3 films in Figs. 7(b) and 7(c), respectively. For the ETP N_2 film in Fig. 7(a), no enhancement of the Si–N absorption peak is visible which might be related to the presence of Si–O absorption bands ($\sim$1070 cm^{-1}) in the spectra. The spectra in Fig. 7(a) show that the film is already oxidized before the high-temperature step takes place and that the Si–O absorption band even increases by the high-temperature step (this takes place in dry air). Si–N bond formation is significantly influenced by oxygen incorporated in the network for this type of film, which can be regarded as silicon oxynitride (a-SiN_xO_y:H).

The H release and film reconstruction as observed in Figs. 6 and 7, indicate that the Si-rich a-SiN_x:H films are less thermally stable than the N-rich a-SiN_x:H films. The ETP N_2 films have a much lower [N]/[Si] ratio for a refractive index $n=\sim$2.1 compared to the ETP NH_3 and MW NH_3 films. The ETP N_2 films might therefore contain a considerable void fraction and the films experience the largest loss in H by the high-temperature step. The difference in thermal stability for the Si-rich and N-rich, which might also be related to the microstructure of the films, is also supported by the change in mass density of the films, as shown in Fig. 8. The mass density increases significantly for the Si-rich films ($x<1.0$) while the mass density of the N-rich films ($x>1.0$) remains relatively unchanged by the high temperature step. Nearly no change in the mass density is observed for the MW NH_3 films revealing a higher degree of thermal stability of these films compared to the ETP N_2 and NH_3 films. This can again be correlated with the higher density of the MW NH_3 films as can be seen from Table III and Fig. 8.

Film densification in combination with a significant loss of H atoms occurs due to the thermal activation as takes

TABLE III. Comparison between the three different as-deposited a-SiN_x:H films with a refractive index n around $\sim$2.1. The films were deposited in ETP N_2–SiH_4, ETP NH_3–SiH_4, and MW NH_3–SiH_4 process.

	ETP N_2	ETP NH_3	MW NH_3
Deposition rate (nm/s)	6.7	3.6	0.7
n (at 2 eV)	2.17	2.03	2.15
E_{04} (eV)	2.55	3.42	3.45
[N] (10^{22} cm^{-3})	2.10 (34.1 at. %)	3.15 (44.2 at. %)	4.22 (50.3 at. %)
[Si] (10^{22} at cm^{-3})	2.65 (43.0 at. %)	2.77 (38.8 at. %)	3.26 (39.0 at. %)
[H] (10^{22} at cm^{-3})	0.95 (15.4 at. %)	1.16 (16.3 at. %)	0.87 (10.5 at. %)
[O] (10^{22} at cm^{-3})	0.46 (7.5 at. %)	0.05 (0.7 at. %)	0.02 (0.2 at. %)
[N]/[Si] ratio	0.79	1.14	1.29
Mass density (g/cm^3)	1.88	2.07	2.53

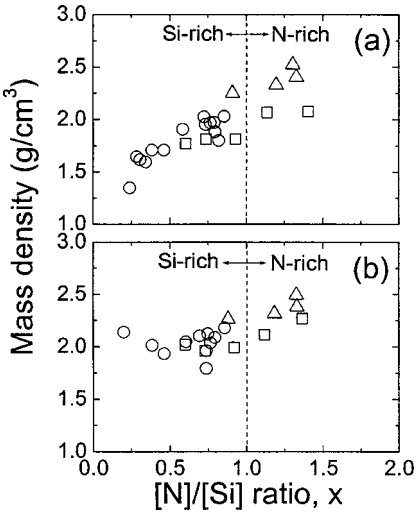

FIG. 8. Changes in mass density of three types of a-SiN_x:H films as a function of the [N]/[Si] ratio x (a) before and (b) after the high-temperature step (○ ETP N_2, □ ETP NH_3, and △ MW NH_3).

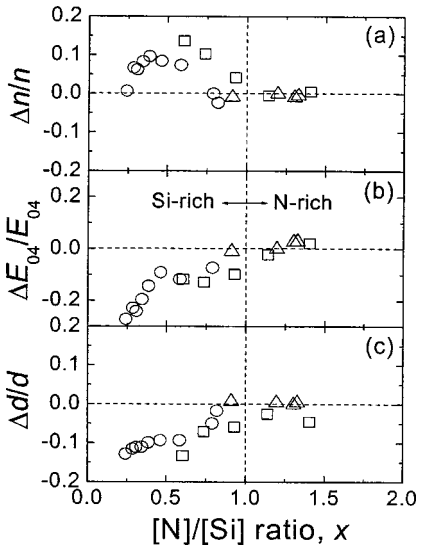

FIG. 9. Relative changes in the optical film parameters of three types of a-SiN_x:H films as a function of the [N]/[Si] ratio due to the high-temperature process step. The relative change of (a) the refractive index $\Delta n/n=(n^A-n^B)/n^B$, (b) the optical band gap $\Delta E_{04}/E_{04}=(E_{04}^A-E_{04}^B)/E_{04}^B$, and (c) the film thickness $\Delta d/d=(d^A-d^B)/d^B$ are presented. The superscripts "*B*" and "*A*" indicate "before" and "after" the high-temperature step, respectively (○ ETP N_2, □ ETP NH_3, and △ MW NH_3).

place during the firing process. Furthermore, densification is a consequence of the decrease in number and size of microscopic voids after the high temperature step. Microscopic voids can, for example, represent the vacant space around H-terminated defects.[42] The loss of H atoms and decrease in microscopic voids lead to a rearrangement and restructuring of the atomic network in the films and as a consequence the average atomic distance between the atoms decreases. Therefore the total atomic density in the film increases while the [N]/[Si] ratio remains approximately constant.

It is observed that the densification due to the high-temperature process step is more pronounced in Si-rich ($x<1.0$) than N-rich ($x>1.0$) a-SiN_x:H films as shown in Fig. 8. The initially less dense Si-rich a-SiN_x:H films experience much more densification. This behavior has been observed before[43] and is in good agreement with the ellipsometric study by Alterovitz *et al.*,[44] who showed that the reduction in void fraction for the Si-rich a-SiN_x:H films was larger than for the N-rich stoichiometric a-SiN_x:H films during rapid thermal annealing.

2. Optical properties

Figure 9 presents the difference in optical film parameters, i.e., the refractive index, optical band gap, and film thickness, of the a-SiN_x:H films before (B) and after (A) the high-temperature step. The relative changes in refractive index (at 2 eV) $\Delta n/n=(n^A-n^B)/n^B$, optical band gap $\Delta E_{04}/E_{04}=(E_{04}^A-E_{04}^B)/E_{04}^B$, and film thickness $\Delta d/d=(d^A-d^B)/d^B$ are given as a function of the [N]/[Si] ratio x of the films. The total thickness d is taken calculated from the spectroscopic ellipsometry data of the bulk layer thickness (d_b) and the surface layer thickness (d_s) by the expression $d=d_b+0.5d_s$.

The results in Fig. 9 show that the refractive index n increases after the high-temperature step for the a-SiN_x:H films in the Si-rich ($x<1.0$) region, while n remains unchanged for the films in N-rich region ($x>1.0$). The optical band gap E_{04} shows a drastic decrease for the Si-rich a-SiN_x:H material while for the near-stoichiometric N-rich a-SiN_x:H films, the optical band gap is even slightly increased (by ~3%) by the high-temperature process step. Both observations can again be explained by the fact that the Si-rich material is less thermally stable than the N-rich a-SiN_x:H. This is also revealed by the decrease in film thickness of the Si-rich a-SiN_x:H films, while the N-rich a-SiN_x:H films remain relatively unaffected, except for the over-stoichiometric ($x=\sim1.4$) ETP NH_3 film.

The distinct influence of the high-temperature process on the optical properties for the Si-rich and N-rich of a-SiN_x:H films can be related to the difference in microstructure of these a-SiN_x:H films. The Si-rich ($x<1.0$) a-SiN_x:H films behave more like a-Si:H films whose properties are dominated by the characteristic Si bond clustering.[39] The a-Si:H-like films have a high refractive index, a narrow band gap and a semi-conducting character and at high temperatures these films lose H atoms (see Fig. 6) and densification occurs. The connectivity of the Si–Si bonds is increased by enhanced Si–Si bond clustering. Consequently, the optical band gap decreases after the high temperature step. On the other hand, the behavior of the N-rich ($x>1.0$) a-SiN_x:H films is quite different from that of the Si-rich counterparts. For the N-rich films, the majority of the bonds in the film network are the stronger Si–N bonds (bond energy: 3.45 eV), which replace the weaker Si–Si bonds (bond energy: 2.34 eV) when the [N]/[Si] ratio increases. The a-SiN_x:H films get a stronger ionic-like covalent Si–N network (similar to a Si–O network) for increasing [N]/[Si] ratio and the stoichiometric silicon nitride (Si_3N_4) is a well-known wide-band-gap (~5.1 eV) and high-density (~3.3 g/cm^3) dielectric material.[39] Therefore, if densification occurs in the dielectric material, the optical band gap can increase while the refractive index increases. Brown *et al.* have observed also an increase in the absorption edge together with an increase in the refractive index for PECVD N-rich a-SiN_x:H films after a rapid thermal anneal.[45] For near-stoichiometric ($x=\sim1.33$) a-SiN_x:H, this unique behavior of the a-SiN_x:H films has also been observed after thermal activation of a-SiN_x:H by ultraviolet irradiation.[42]

IV. DISCUSSION ON THE EFFECT OF THE FILM PROPERTIES ON THE BULK PASSIVATION OF MULTICRYSTALLINE SILICON SOLAR CELLS

In this section, the observations addressed in Sec. III will be related to previously reported experiments in which the performance of the a-SiN_x:H films with respect to bulk passivating antireflection coatings on multicrystalline silicon so-

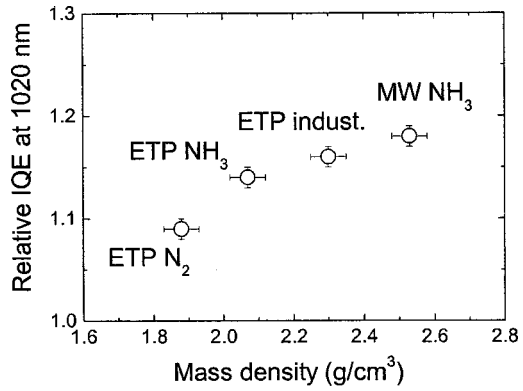

FIG. 10. Relative internal quantum efficiency (IQE) of the a-SiN_x:H coated mc-Si solar cells measured at 1020 nm as a function of the mass density of the a-SiN_x:H films. The values are taken relative with respect to solar cells coated with an a-SiN_x:H antireflection coating but without bulk passivation (see Ref. 17). The film properties of the three a-SiN_x:H films are listed in Table III. Furthermore, the relative IQE value and the corresponding mass density is given for a solar cell with a-SiN_x:H film (refractive index $\sim$2.1), which is deposited at high rate by an industrial-type ETP reactor (ETP indust.). The relative IQE values can directly be compared with each other because the solar cells have been manufactured form neighboring wafers from the same ingot and have undergone the same processing apart from the deposition of the a-SiN_x:H.

lar cells has been investigated.[17] From this more insight into the mechanism of bulk passivation of solar cells by a-SiN_x:H can be obtained.

The three types of the a-SiN_x:H films described in Table III have been applied to industrial-type mc-Si solar cells as bulk-passivating AR coatings. The specific deposition conditions have been chosen such that a refractive index of $\sim$2.1 at 2 eV and a film thickness of $\sim$75 nm is obtained. Generally, these film parameters yield an "optimized" single AR layer on the n^+ p-type mc-Si cells (10×10 cm^2 size, 330 μm thick). The bulk passivation of the mc-Si solar cells by the a-SiN_x:H films as induced by the firing process has been investigated by analyzing the internal quantum efficiency (IQE) of the cells. As also reported previously,[17,18] bulk passivation has been observed for all three types of a-SiN_x:H films as concluded from an enhancement of the IQE at long wavelengths (red response) compared to cells without bulk passivation. However, the degree of bulk passivation depends on the type of a-SiN_x:H applied as shown in Fig. 10. Figure 10 shows the relative IQE at 1020 nm for the three different a-SiN_x:H films on mc-Si solar cells as a function of the mass density of the a-SiN_x:H films. Because the mc-Si solar cells have been manufactured from neighboring wafers from the same ingot and have undergone the same processing, the relative IQE values can directly be compared with each other. Figure 10 suggests therefore that the degree of bulk passivation increases with increasing density of the a-SiN_x:H films.

The correlation between bulk passivation and the film mass density as suggested by Fig. 10 implies that a larger loss of H atoms from the a-SiN_x:H film by the firing process does not simply lead to a higher degree of bulk passivation in the mc-Si cells. For the ETP N_2 films, which show the largest loss in H concentration, the hydrogen species probably diffuse mainly out into the ambient instead of diffusing into the mc-Si material to passivate defects. This diffusion into the ambient is most probably facilitated by the lower mass density of the ETP N_2 films compared to the ETP NH_3 and MW NH_3 films and the related porous microstructure. Moreover, the results show that the hydrogen atomic density in the as-deposited a-SiN_x:H film is not directly related to the degree of bulk passivation obtained. Apparently, not the amount of hydrogen but the process of out-/in-diffusion determines the degree of bulk passivation obtained by the SiN_x:H film after firing. Consequently, a high atomic density and high thermal stability of the a-SiN_x:H film appears to be one of the factors which are important for obtaining a high level of bulk passivation. A high thermal stability of a-SiN_x:H films has also been reported to be important for high quality surface passivation of silicon.[46]

More evidence for the relation between the atomic density of the a-SiN_x:H film and the degree of bulk passivation is provided by an experiment in which an industrial-type of ETP reactor has been used.[47] As indicated in Fig. 10, a solar cell coated with a-SiN_x:H by this reactor revealed a higher degree of bulk passivation while the mass density of the a-SiN_x:H (refractive index $\sim$2.1) was also higher than for the other ETP deposited films described in this article. Furthermore, this experiment revealed that the bulk passivation quality obtained by the ETP technique is nearly as good as achieved with the ECN microwave technique.

Finally, we want to remark that a possible influence of aluminum-enhanced diffusion of hydrogen into the Si has not been addressed in this study. In the literature, it has been reported that the simultaneous firing process step of the a-SiN_x:H and the formation of an Al back surface field on the back of solar cells enhances the hydrogen passivation of the bulk defects.[13,15] This effect might have taken place during the production of the solar cells (containing an Al back surface field)[17] discussed in this section, but has not been studied in Sec. III in which the influence of the high-temperature step on the a-SiN_x:H properties has been investigated.

V. CONCLUSIONS

The influence of the so-called firing process on the compositional and optical properties of high-rate remote plasma deposited silicon nitride films has been investigated. These a-SiN_x:H films have an important application as antireflection coatings on mc-Si solar cells in which the firing of the metallization through the silicon nitride film leads to bulk passivation of the defects in the mc-Si. Three types of remote plasma deposited a-SiN_x:H films have, therefore, been investigated before and after a high-temperature step that mimics the firing process: expanding thermal plasma deposited a-SiN_x:H films from a N_2-SiH_4 gas mixture, ETP deposited a-SiN_x:H films from a NH_3-SiH_4 mixture, and microwave plasma deposited a-SiN_x:H films from a NH_3-SiH_4 mixture. It has been observed that the high-temperature step can result in significant changes in the film properties. Hydrogen

is released from the films and the atomic density of Si and N atoms increases while the [N]/[Si] ratio remains constant. This densification, which decreases the film thickness, is caused by a structural rearrangement of the film's network creating more Si–N bonds and leading to a higher refractive index. These thermally induced changes are most pronounced for Si-rich a-SiN_x:H films and they are nearly absent for the N-rich a-SiN_x:H films. The increase of refractive index by the high temperature process step leads also to a decrease in optical band gap for the Si-rich films and an increase in optical band gap for the N-rich films. The N-rich films deposited by the MW NH_3-SiH_4 plasma, which have the highest atomic density show, however, almost no change after the high temperature step. These films have the highest thermal stability and this seems to be correlated to the high degree of bulk passivation in mc-Si solar cells obtained by these a-SiN_x:H films. The results on the three different a-SiN_x:H films suggest that the passivation quality is related to the material properties of the as-deposited a-SiN_x:H films in which a high atomic density and high thermal stability of the films seem to be two important factors for obtaining a high degree of bulk passivation.

ACKNOWLEDGMENTS

This study has been carried out within the E.E.T.-program ''Sunovation'' funded by the Netherlands Ministry of Economic Affairs, the Ministry of Education, Culture and Science and the Ministry of Public Housing, Physical Planning and Environment. M. J. F. van de Sande, J. F. C. Jansen, A. B. M. Hüsken, H. M. M. de Jong, H. C. Rieffe, E. J. Kossen, M. Koppes, and H. G. ter Beeke are acknowledged for their skilful technical assistance.

[1]J. T. Milek, *Silicon Nitride for Microelectronic Applications, Part 2: Applications and Devices, Handbook of Electronic Materials* (IFI/Plenum, New York, 1972), Vol. 6.
[2]V. I. Belyi, L. L. Vasilyeva, A. S. Ginkvker, V. A. Gritsenko, S. M. Repinsky, S. P. Sinitsa, T. P. Smirnova, and F. L. Edelman, *Silicon Nitride in Electronics, Material Science Monographs* (Elsevier, Amsterdam, 1988), p. 34.
[3]A. G. Aberle, T. Lauinger, and R. Hezel, Proceedings of the 14th European Photovoltaic Solar Energy Conference, Barcelona, Spain (1997), p. 684.
[4]P. Doshi, G. E. Jellison, Jr., and A. Rohatgi, Appl. Opt. **36**, 7826 (1997).
[5]S. Winderbaum, F. Yun, and O. Reinhold, J. Vac. Sci. Technol. A **15**, 1020 (1997).
[6]A. G. Aberle, Sol. Energy Mater. Sol. Cells **65**, 239 (2001).
[7]F. Duerinckx and J. Szlufcik, Sol. Energy Mater. Sol. Cells **72**, 231 (2002).
[8]J. Schmidt and M. Kerr, Sol. Energy Mater. Sol. Cells **65**, 585 (2001).
[9]R. Lüdemann, Mater. Sci. Eng., B **58**, 86 (1999).
[10]W. M. Arnoldbik, R. N. H. Linssen, F. H. P. M. Habraken, W. F. van der Weg, and A. E. T. Kuiper, Appl. Phys. Lett. **56**, 2530 (1990).
[11]C. Boehme and G. Lucovsky, J. Appl. Phys. **88**, 6055 (2000); J. Vac. Sci. Technol. A **19**, 2622 (2001); J. Non-Cryst. Solids **299-302**, 1157 (2002).
[12]B. L. Sopori, X. Deng, J. P. Benner, A. Rohatgi, P. Sana, S. K. Estreicher, Y. K. Park, and M. A. Roberson, Sol. Energy Mater. Sol. Cells **41/42**, 159 (1996).
[13]J.-W. Jeong, M. D. Rosenblum, J. P. Kalejs, and A. Rohatgi, J. Appl. Phys. **87**, 7551 (2000).
[14]L. Cai, A. Rohatgi, D. Yang, and M. A. El-Sayed, J. Appl. Phys. **80**, 5384 (1996).
[15]V. Yelundur, A. Rohatgi, A. Ebong, A. M. Gabor, J. Hanoka, and R. L. Wallace, J. Electron. Mater. **30**, 526 (2001).
[16]A. Rohatgi, V. Yelundur, J. Jeong, A. Ebong, M. D. Rosenblum, and J. I. Hanoka, Sol. Energy Mater. Sol. Cells **74**, 117 (2002).
[17]J. Hong, W. M. M. Kessels, F. J. H. van Assche, H. C. Rieffe, W. J. Soppe, A. W. Weeber, and M. C. M. van de Sanden, Prog. Photovoltaics **11**, 125 (2003).
[18]J. Hong, W. M. M. Kessels, F. J. H. van Assche, W. M. Arnoldbik, H. C. Rieffe, W. J. Soppe, A. W. Weeber, and M. C. M. van de Sanden, Proceedings of the 29th IEEE Photovoltaic Specialists Conference, New Orleans (2002), p. 154.
[19]W. M. M. Kessels, J. Hong, F. J. H. van Assche, M. D. Moschner, T. Lauinger, W. J. Soppe, A. W. Weeber, D. C. Schram, and M. C. M. van de Sanden, J. Vac. Sci. Technol. A **20**, 1704 (2002).
[20]W. M. M. Kessels, R. J. Severens, A. H. M. Smets, B. A. Korevaar, G. J. Adriaenssens, D. C. Schram, and M. C. M. van de Sanden, J. Appl. Phys. **89**, 2404 (2001).
[21]W. M. M. Kessels, F. J. H. van Assche, J. Hong, J. D. Moschner, T. Lauinger, D. C. Schram, and M. C. M. van de Sanden, Mater. Res. Soc. Symp. Proc. **664**, A8.6.1 (2001).
[22]W. J. Soppe, C. Devilée, S. E. A. Schiermeier, J. Hong, W. M. M. Kessels, M. C. M. van de Sanden, W. M. Arnoldbik, and A. W. Weeber, Proceedings of the 17th European Photovoltaic Solar Energy Conference and Exhibition, Munich, Germany (2001), p. 1543.
[23]W. J. Soppe, B. G. Duijvelaar, S. E. A. Schiermeier, A. W. Weeber, A. Steiner, and F. M. Schuurmans, Proceedings of the 16th European Photovoltaic Solar Energy Conference, Glasgow, U.K. (2000), p. 1420.
[24]W. J. Soppe, J. Hong, W. M. M. Kessels, M. C. M. van de Sanden, W. M. Arnoldbik, H. Schlemm, C. Devilée, H. Rieffe, S. E. A. Schiermeier, J. H. Bultman, and A. W. Weeber, Proceedings of the 29th IEEE Photovoltaic Specialists Conference, New Orleans (2002), p. 158.
[25]W. M. Arnoldbik and F. H. P. M. Habraken, Rep. Prog. Phys. **56**, 859 (1993).
[26]C. H. M. Marée, A. M. Vredenberg, and F. H. P. M. Habraken, Mater. Chem. Phys. **46**, 198 (1996).
[27]G. E. Jellison, Jr. and F. A. Modine, Appl. Phys. Lett. **69**, 371 (1996); **69**, 2137 (1996).
[28]S. Lee and J. Hong, Jpn. J. Appl. Phys., Part 1 **39**, 241 (2000).
[29]J. Hong, A. Goullet, and G. Turban, Thin Solid Films **352**, 41 (1999).
[30]J. W. A. M. Gielen, D. C. Schram, and M. C. M. van de Sanden, Thin Solid Films **271**, 56 (1995).
[31]F. Demichelis, F. Giorgis, and C. F. Pirri, Philos. Mag. B **74**, 155 (1996).
[32]S. Hasegawa, L. He, Y. Amano, and T. Inokuma, Phys. Rev. B **48**, 5315 (1993).
[33]W. S. Liao, C. H. Lin, and S. C. Lee, Appl. Phys. Lett. **65**, 2229 (1994).
[34]D. L. Smith, A. S. Alimonda, and F. J. von Preissig, J. Vac. Sci. Technol. B **8**, 551 (1990).
[35]D. L. Smith, A. S. Alimonda, C.-C. Chen, S. E. Ready, and B. Wacker, J. Electrochem. Soc. **137**, 614 (1990).
[36]D. L. Smith, J. Vac. Sci. Technol. A **11**, 1843 (1993).
[37]W. M. M. Kessels, F. J. H. van Assche, J. Hong, D. C. Schram, and M. C. M. van de Sanden, J. Vac. Sci. Technol (submitted).
[38]G. Lucovsky, J. Vac. Sci. Technol. **16**, 1225 (1979).
[39]J. Robertson, Philos. Mag. B **69**, 307 (1994).
[40]Z. Lu, P. Santos-Filho, G. Stevens, M. J. Williams, and G. Lucovsky, J. Vac. Sci. Technol. A **13**, 607 (1995).
[41]P. Santos-Filho, G. Stevens, Z. Lu, K. Koh, and G. Lucovsky, Mater. Res. Soc. Symp. Proc. **398**, 3102 (1996).
[42]H. Akazawa, Appl. Phys. Lett. **80**, 3102 (2002).
[43]C. M. M. Denisse, K. Z. Troost, F. H. P. M. Habraken, and W. F. van der Weg, J. Appl. Phys. **60**, 2543 (1986).
[44]S. A. Alterovitz, M. A. Drotos, and P. G. Young, Mater. Res. Soc. Symp. Proc. **284**, 45 (1993).
[45]W. D. Brown and M. A. Khaliq, Thin Solid Films **186**, 73 (1990).
[46]B. Lenkeit, S. Steckemetz, F. Artuso, and R. Hezel, Sol. Energy Mater. Sol. Cells **65**, 317 (2001).
[47]M. Bijker, private communication (2002).